JOURNAL OF Materials CHEMISTRY

Synthesis, crystal structures, electronic structure and magnetic behaviour of the trithiatriazapentalenyl radical, $C_2S_3N_3$†

Gordon D. McManus,[a] Jeremy M. Rawson,*[a] Neil Feeder,[a] Joost van Duijn,[a] Eric J. L. McInnes,[b] Juan J. Novoa,[c] Ramon Burriel,[d] Fernando Palacio*[d] and Patricia Oliete[d]

[a]*Department of Chemistry, The University of Cambridge, Lensfield Road, Cambridge, UK CB2 1EW. E-mail: jmr31@cam.ac.uk*
[b]*EPSRC* c.w. *EPR Service Centre, Department of Chemistry, University of Manchester, Oxford Road, Manchester, UK M13 9PL*
[c]*Departmento de Quimica Fisica and CER Quimica Teorica, Universidad de Barcelona, Av. Diagonal 647, 08028 Barcelona, Spain*
[d]*Instituto de Ciencia de Materiales de Aragon, CSIC Universidad de Zaragoza, E-50009 Zaragoza, Spain*

Received 6th April 2001, Accepted 17th April 2001
First published as an Advance Article on the web 14th June 2001

A novel synthesis of the title compound, $C_2S_3N_3$ (**1**) is reported. X- and K-band EPR spectra on dilute solutions of **1** indicate delocalisation of the unpaired spin density over both heterocyclic rings in agreement with DFT calculations. An XRPD study indicates that it crystallises in two morphologies with both phases formed during vacuum sublimation. The XRPD studies indicate that on cooling below 230 K, only the triclinic phase ($P\bar{1}$) becomes detectable, whereas on warming above 320 K, just the monoclinic phase ($P2_1/c$) becomes observed. The crystal structure of the monoclinic phase has been examined by variable temperature single crystal X-ray diffraction in the region 300–225 K and reveals a regular π-stacked structure. A crystal structure of the triclinic phase is reported at 150 K and exhibits a dimeric π-stacked motif. Susceptibility measurements show that the monoclinic phase is paramagnetic whereas the triclinic phase is diamagnetic. This radical exhibits thermal hysteresis with a wide range of bistability; EPR and magnetic susceptibility measurements indicate $Tc_{\downarrow} = 234$ K, and $Tc_{\uparrow} = 317$ K. The magnetic behaviour of the monoclinic phase is consistent with strong antiferromagnetic exchange interactions between open shell doublet states ($J = -320$ K) along the **π**-stacking direction, although significant inter-stack interactions are required to model the data adequately. In contrast the dimeric phase is essentially diamagnetic, with the residual paramagnetism indicating a very large singlet–triplet separation ($|2J| > 2000$ K). The magnetic exchange interactions in both phases are probed through a series of DFT calculations using the broken-symmetry approach. These confirm the presence of strong magnetic exchange interactions along the **π**-stacking direction in the high temperature phase ($2J = -182$ K), but with additional interstack interactions which are an order of magnitude smaller. Calculations on the triclinic phase indicate that it is best considered as a dimer with an open-shell singlet state with a very large singlet–triplet separation ($2J = -2657$ K). The magnitude of J for both phases from theory and experiment are in good agreement. The origin of the thermal hysteresis is attributed to the presence of two energetically similar structures which have a low energy barrier to interconversion. The thermodynamic parameters associated with the interconversion process have been probed by DSC studies. It confirms the first order nature of the transition with $Tc_{\downarrow} = 232.3$ K ($\Delta H_{\downarrow} = 1.41$ kJ mol^{-1}, $\Delta S_{\downarrow} = 6.0$ J mol^{-1} K^{-1}) and $Tc_{\uparrow} = 320.5$ K ($\Delta H_{\uparrow} = 1.86$ kJ mol^{-1}, $\Delta S_{\uparrow} = 5.8$ J mol^{-1} K^{-1}).

Introduction

We have been interested for some time in the development of thiazyl radicals as molecular magnetic materials.[1–3] The lack of steric hindrance in these systems affords close approach of the radical centres which leads to large magnetic exchange interactions between radical centres, evidenced by Weiss constants with magnitudes up to 10^2 K. This has culminated in the observation of weak ferromagnetism in the dithiadiazolyl radical, **2**, at 36 K at ambient pressure.[2] The application of pressure leads to a further enhancement of T_c to 51 K at 7 kbar,[4] the highest T_c for an open shell organic radical. However the large enthalpy of dimerisation ($\sim$35 kJ mol^{-1})[5] for these derivatives makes the design of paramagnetic derivatives arduous and we have begun to examine dithiazolyl radicals, **3**, in which the dimerisation enthalpy is small ($\sim$0 kJ mol^{-1}).[6]

Work by us[7] and others[8–10] has shown that a number of dithiazolyl radicals are monomeric in the solid state. The

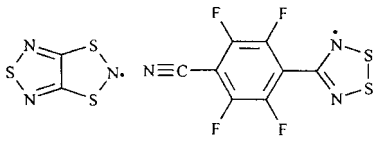

1 **2**

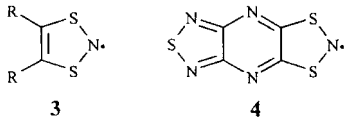

3 **4**

†Electronic supplementary information (ESI) available: pdb files of the solid state structures of the high and low temperature phases of **1**. See http://www.rsc.org/suppdata/jm/b1/b103303b/

 DOI: 10.1039/b103303b

magnetic behaviour of the derivative **4** was reported[10] to exhibit bistability in which both paramagnetic and antiferromagnetic phases are stable between 50 and 200 K. As a continuation of our own work in this area, we investigated the fused radical **1**, first reported by Wolmershauser.[11] During the course of our investigations, Awaga and Fujita published a report[12] on the bistability of **1** at room temperature and the observation of thermal hysteresis between 230 and 305 K. Although the crystal quality of the high temperature (monoclinic) phase appeared poor (on the basis of the errors in the unit cell parameters), the structures of the two phases were clearly established at room temperature. In their studies they indicated that the spin density distribution is localised on the SNS fragment of the dithiazolyl ring. In addition, the magnetic susceptibility was proposed to be one-dimensional, despite their modelling of the magnetic data with a very strong mean field correction to account for inter-stack interactions. The ratio of interstack/intrastack interaction is *ca.* 0.2. The bistability was attributed to a cooperative interaction between spin-Peierls instability and strong inter-stack interactions, such that the competition between exchange and electrostatic terms provide a potential energy barrier to interconversion.

Here we report our own studies on this system. We present a novel synthesis of **1** and probe its detailed electronic structure through a combination of solution EPR and DFT calculations. These clearly show π-delocalisation of the spin density over the entire molecule. We provide a detailed study of the structure of **1** through a combination of X-ray powder diffraction (XRPD) and variable temperature single crystal X-ray diffraction. The variable temperature single crystal data on the monoclinic phase indicates a slight preference for a contraction of the crystal lattice along the π-stacking direction. The XRPD data shows that no intermediate ternary phase appears present. We have also probed the region of bistability in **1** through X-ray diffraction, magnetisation and EPR studies and differential scanning calorimetry (DSC) measurements. Our data consistently exhibit a wider range of bistability, 234–317 K, *ca.* 10% larger than that previously reported. In addition, we report the first theoretical studies on the magnetic exchange interactions in **1** through DFT studies. The bistability is rationalised in terms of two polymorphs with a small energy barrier to interconversion.

Results

Synthesis

Radical **1** was originally prepared[11] from dichlorothiadiazole, **5**, according to Method **A** in Scheme 1. In our hands, the reaction of **5** with Na_2S (or Li_2S) proved problematic and we sought an alternative route to the intermediate salt, **6**. Condensation of dithiooxamide with SCl_2, followed by chlorination with SO_2Cl_2 yielded a bis(sulfenyl chloride) which underwent ring closure with Me_3SiN_3 to form **6** reliably in 39% yield (Method **B**). Subsequent reduction of **6** with $Na_2S_2O_4$ produced **1** which could be recovered analytically pure in moderate yield (30%) by vacuum sublimation (10^{-2} Torr, 60 °C).

Electronic structure of 1

EPR studies. Solution EPR studies on **1** were performed on a CH_2Cl_2 : toluene (*ca.* 10 : 1 v/v) mixture. The observed line-width in fluid solution at room temperature was strongly concentration dependent and narrowed in degassed solvents. Solutions used for all subsequent experiments were degassed and diluted to the point at which there was no improvement in line-width. At room temperature, **1** exhibited a well-defined 1 : 1 : 1 triplet spectrum ($g_{iso} = 2.0053$, $a_{iso}^{N(1)} = 11.2$ G) consistent with coupling to the unique ^{14}N atom, N(1). No resolution

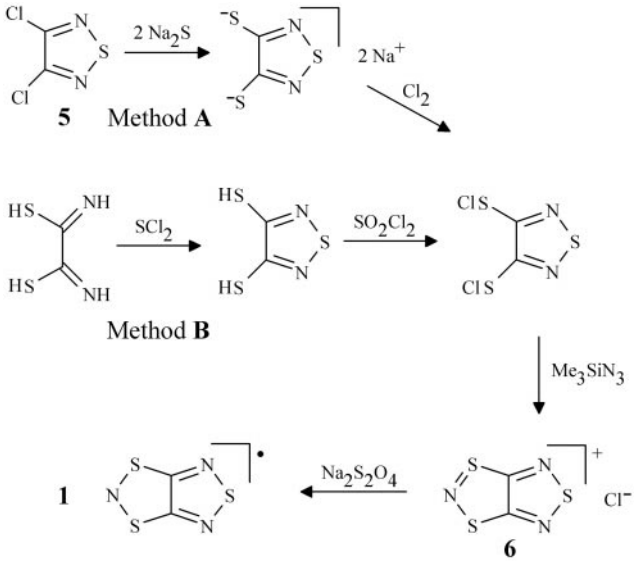

Scheme 1 Synthetic route to **1**.

of hyperfine coupling to the two N(2) atoms was observed and there was no improvement in resolution in the temperature range 300–240 K. Simulation of the line-shape of the isotropic spectrum utilised a small coupling constant to the two equivalent N(2) atoms ($a_{iso}^{N(2)} = 0.7$ G); this value is consistent with those determined from frozen solutions (*vide infra*), although the error could be considerable. These values are comparable with those reported by Sutcliffe and co-workers ($g = 2.00611$, $a_{iso}^{N(1)} = 11.15$ G, $a_{iso}^{N(2)} = 0.84$ G, $a_{iso}^{S(1)} = 3.29$ G recorded in d_8-toluene at 213 K).[13]

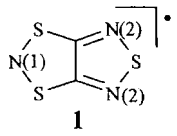

Frozen solutions at *ca.* 100 K exhibited rhombic EPR spectra ($g_1 \neq g_2 \neq g_3$,). Only the smallest *g*-value (g_1) exhibited an observable hyperfine coupling pattern (Fig. 1): a triplet to the unique N(1) ($a_1^{N(1)} = 28.4$ G), further split into 1 : 2 : 3 : 2 : 1 pentets by a smaller coupling to the two equivalent N(2) nuclei of the thiadiazole ring ($a_1^{N(2)} = 2.5$ G). The central pentet of the

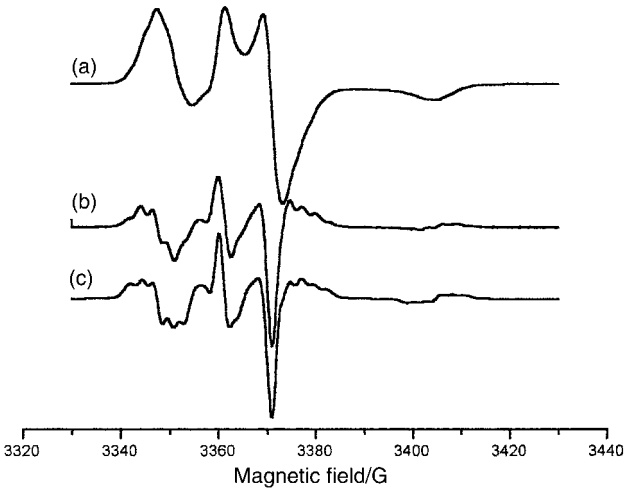

Fig. 1 (a) First derivative and (b) second derivative frozen solution X-band EPR spectrum ($\nu = 9.447$ GHz) of **1** in (CH_2Cl_2–toluene) at 103 K; (c) simulation using parameters given in Table 1.

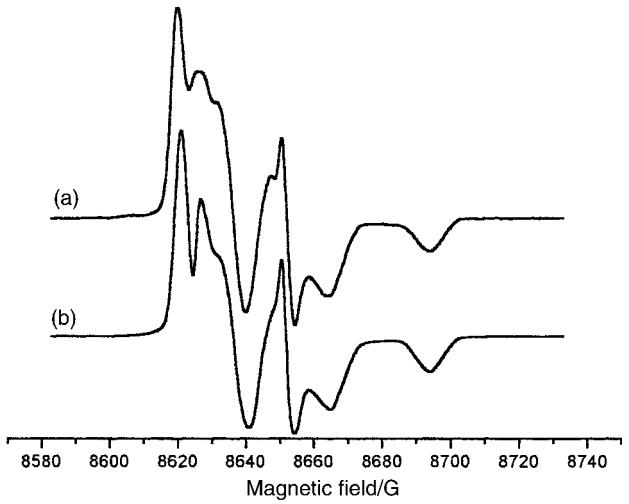

Fig. 2 Frozen solution K-band EPR spectrum ($\nu = 24.206$ GHz) of **1** in (CH_2Cl_2–toluene) at 117 K; (a) experimental; (b) simulation. Note the intense undershoot resonance at low field.

triplet overlaps with the central g_2 resonance. The N(2) hyperfine structure on g_1 is resolved clearly in the second derivative X-band spectrum (Fig. 1b). Hyperfine structure to N(1) or N(2) is not observed on g_2 or g_3 implying much smaller coupling constants than those observed on g_1. The K-band spectrum provides the expected improvement in resolution of the *g*-values: note that the N(2) splittings on g_1 are now unresolved (Fig. 2a). An interesting spectroscopic feature is the lowest-field resonance at K-band. This could easily be mistaken for a principal *g*-value: however, simulations reveal that it is an off-axis "undershoot" resonance.[14] The spin-Hamiltonian parameters are confirmed by successful simulation of the frozen solution X- and K-band spectra with the *same* set of parameters, barring minor changes in line-width (Figs. 1c and 2b). Small hyperfine couplings to both N(1) and N(2) on g_2 and g_3 were incorporated to optimise fits to the experimental line-shapes. The errors on these small couplings are likely to be large, but their impact on the spin-density calculations (described below) is rather small. A summary of both the isotropic and anisotropic EPR data is provided in Table 1. The parameters reported by Sutcliffe and co-workers are included for comparison.[13] The lack of hyperfine structure to g_2 and g_3, coupled with g_1 exhibiting a value close to that for the free electron, is entirely consistent with the unpaired electron residing in a π-type orbital with g_1 coparallel to the direction perpendicular to the plane of the molecule. This is supported by the values of the isotropic hyperfine interactions when converted into s-orbital unpaired spin density populations (*vide infra*) and is in agreement with other studies on dithiazolyl radicals[13,15] and related systems.[16]

Calculated spin density distribution. Analysis of the hyperfine coupling parameters from isotropic and anisotropic solution spectra has proved to be a useful technique for mapping the spin density distributions in heterocyclic π-radicals.[17] The isotropic s-orbital spin density (ρ_s) at N(1) and N(2) can be simply estimated by comparison of the observed hyperfine interactions (in MHz: see Table 1) with the theoretical parameter, *A*, obtained by Morton and Preston,[18] according to eqn. (1):

$$\rho_s = \frac{a_{iso} \times 100}{A} \quad (1)$$

The π spin density can be estimated from a comparison of the anisotropic hyperfine interactions (in MHz), with the corresponding theoretical parameter, *P* (eqn. (2)):[18]

$$\rho_\pi = \frac{[a_3 - 1/2(a_2 + a_1)] \times 100}{3P} \quad (2)$$

Errors on the s-electron density were estimated by examining the results obtained using both a_{iso} and the average of the anisotropic data, $<a>$ and were within 0.1%. Errors on π-electron density were estimated assuming that the hyperfine interactions could be of the same or different signs, and were also within 0.1%. A summary of the calculated s and π spin density distributions are presented in Table 2 and compare very well with those reported previously[13] and with the total spin density distributions determined from the DFT calculations described below.

DFT calculations. Previous attempts[13] to calculate both isotropic and anisotropic hyperfine interactions using semi-empirical methods (MNDO and INDO) were unsuccessful. Spin anihilation gave rise to large errors in calculated *p*-electron densities. More recent work by Gassmann and Fabian[19] has shown that the DFT-optimised geometries of thiazyl radicals are in rather poor agreement with observed

Table 1 Isotropic and anisotropic EPR parameters for **1**. Values marked * are estimates based on simulation; these superhyperfine couplings were not resolved

g-matrix			G	MHz		G	MHz
g_1	2.0015	$a_1^{N(1)}$	28.4	79.55	$a_1^{N(2)}$	2.5	7.00
g_2	2.0046	$a_2^{N(1)}$	~2*	~5.61*	$a_2^{N(2)}$	~0.2*	~0.56*
g_3	2.0105	$a_3^{N(1)}$	~2*	~5.63*	$a_3^{N(2)}$	~0.2*	~0.56*
$<g>$	2.0055	$<a^{N(1)}>$	10.8	30.31	$<a^{N(2)}>$	1.0	2.81
g_{iso}	2.0053	$A_{iso}^{N(1)}$	11.2	31.43	$a_{iso}^{N(2)}$	~0.7	1.96

Table 2 Theoretical spin density distribution determined from DFT calculation and calculated spin density distributions at the heterocyclic N atoms from EPR data. The atom labelling scheme follows that given in the text

	% s-electron density		% π-electron density		% total spin density	
Atom	DFT	EPR	DFT	EPR	DFT	EPR
N(1)	—	1.7	47.6	44.4	50.7	46.1
S(1)	—	—	14.2	—	16.7	—
C	—	—	−1.9	—	−3.1	—
N(2)	—	0.1	5.6	3.9	5.7	4.0
S(2)	—	—	9.9	—	11.1	—

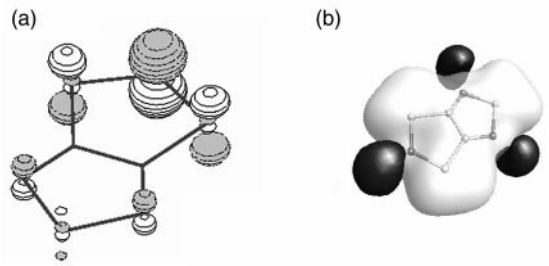

Fig. 3 (a) Singly occupied molecular orbital and (b) molecular electrostatic potential (MEP) map for **1** (dark regions -10 kcal mol^{-1}, light regions $+10$ kcal mol^{-1}.

data (in comparison to closed-shell N-free, sulfur heterocycles) and tend to over-estimate bond lengths, although reasonable agreements were observed between theoretical and experimental hyperfine coupling constants.

Our DFT calculations were carried out on **1** using the molecular geometry determined from the single crystal studies reported by Wolmershauser.[11] These calculations indicate that the unpaired electron resides in a π^* orbital which is delocalised over the entire molecule (Fig. 3a). However, the spin density distribution is asymmetric with 84% based on the SNS fragment and just 22% on the NSN fragment. The slight excess of spin density on the heteroatoms, N and S, is compensated by a small (3%) negative spin density at each C. A comparison of the theoretical and calculated spin densities at N (Table 2) indicates an excellent agreement and provides a firm basis for interpreting the magnetic behaviour of **1** (see below). Importantly, the delocalisation of π-spin density suggests that intermolecular interactions between both dithiazolyl and thiadiazolyl rings may be important in propagating the magnetic exchange interactions.

X-Ray diffraction studies on 1

Crystals of **1** could be grown by vacuum sublimation (60 °C, 10^{-2} Torr). Radical **1** was found to be polymorphic, crystallising in either of two structural modifications: a monoclinic phase ($P2_1/c$) and a triclinic phase ($P\bar{1}$). The structure of **1** was probed by a combination of XRPD and single crystal measurements.

X-Ray powder diffraction. XRPD studies on the sublimed material showed both polymorphs are present in an approximately 50 : 50 mole ratio. The two polymorphs are readily discernible by the positions of their two intense, low angle, reflections ($2\theta = 16.587$ and $18.382°$ for the triclinic phase and 17.393 and $19.445°$ for the monoclinic phase). After quenching the as-prepared sample in liquid nitrogen (77 K), the XRPD pattern recorded at room temperature showed only the presence of the triclinic phase. Subsequent warming to 328 K for 2 hours, produced the monoclinic phase. The XRPD patterns for the as-prepared sample, and after subsequent cooling and heating cycles are shown in Fig. 4. The XRPD patterns of the low temperature triclinic and high temperature monoclinic phases were confirmed by simulation using crystallographic data from single crystal studies (below). No evidence for a ternary phase was detectable in any of these XRPD measurements, indicating a simple, reversible, interconversion between the two phases.

High temperature phase. The crystal structure of the high temperature phase was originally reported by Wolmershauser[11] and more recently a room temperature structure was reported[12] by Awaga. In the latter case the large errors on the unit cell parameters possibly indicate poor crystal quality, although the residuals in the last stages of refinement seem satisfactory. We reinvestigated the high temperature phase in order to examine any subtle changes in geometry or intermolecular contacts which might occur, particularly close to the phase transition temperature. There are no significant deviations between the present data and previous determinations, although the current report allows us to investigate the temperature dependence of the intermolecular contacts. The crystal structure of the high temperature phase was examined on the same single crystal of **1** at 310 K, 250 K and, around the low temperature phase transition (determined by magnetic studies, *vide infra*), at 225 K. Throughout this temperature range **1** was found to be monoclinic ($P2_1/c$).

At 310 K, the molecular structure of **1** (Fig. 5a) is planar within 0.0025 Å and is of unexceptional geometry. The molecules form a regular π-stack along the crystallographic *b*-axis and are inclined at 21° to the stacking direction (Fig. 5b). Work by Nyburg and Faerman[20] has shown that the van der Waals radii of S is aspherical. In our case significant S···S

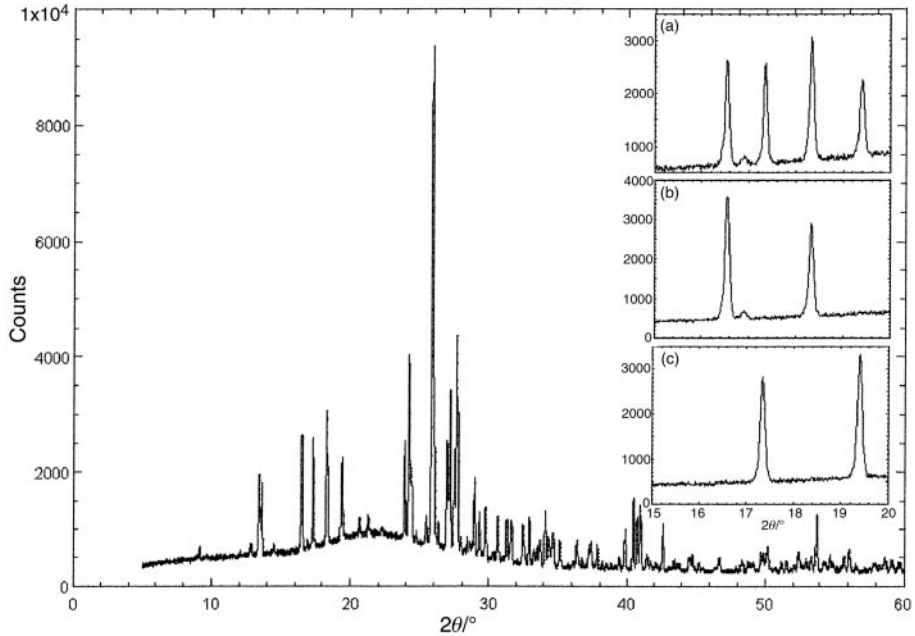

Fig. 4 XRPD pattern of **1** as prepared. Inset low angle data ($15 < 2\theta < 20°$) for the sample (a) as prepared, (b) on quenching to 77 K and (c) after warming to 50 °C for 2 h.

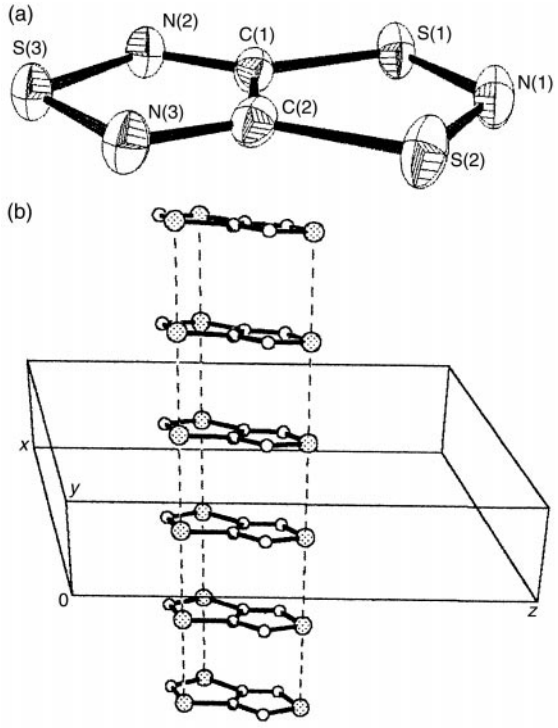

Fig. 5 (a) The asymmetric unit of **1** (monoclinic phase) at 225 K; (b) regular packing of **1** along the stacking direction in the high temperature phase. Selected bond lengths and angles are, at 225 K: S(1)–N(1) 1.655(2), S(1)–C(1) 1.736(2), S(2)–N(1) 1.657(2), S(2)–C(2) 1.734(2), S(3)–N(2) 1.648(2), S(3)–N(3) 1.648(2), N(2)–C(1) 1.316(3), N(3)–C(2) 1.317(3), C(1)–C(2)1.435(3) Å; C(1)S(1)(N1) 98.17(10), C(2)S(2)N(1) 97.96(10), N(2)S(3)N(3) 99.16(9), S(1)N(1)S(2) 116.78(11), C(1)N(2)S(3) 106.26(15), C(2)N(3)S(3) 106.40(15), C(2)C(1)N(2) 114.27(20), C(2)C(1)S(1) 113.32(17), C(1)C(2)N(3) 113.91(21), C(1)C(2)S(2) 113.77(17)°.

contacts along the stacking direction are expected to be less than 4.06 Å, with significant in plane S···S and S···N contacts in the region of 3.20 Å. The intra-stack separation is equivalent to the length of the crystallographic *b*-axis, 3.717 Å, significantly less than the sum of the van der Waals radii perpendicular to the ring plane. A web of interstack contacts between molecules of **1** also exist; whilst the majority are in excess of the sum of the van der Waals radii in the ring plane (3.2 Å), a number are less than this value. These comprise S···N contacts, the closest of which are S(2a)···N(3g) at 3.031 Å, with S(3a)···N(2e) at 3.115 Å, S(3a)···N(1p) at 3.138 Å [and S(2a)···N(1k) at 3.237 Å] (Fig. 6).

Some contraction of the crystal lattice was detectable on cooling from 310 to 225 K (see Table 3) with slightly more contraction along the stacking axis (the crystallographic *b* axis), than *a* or *c* axes. The molecular structure was essentially identical at all temperatures, but with a small decrease in the uncertainty of the atomic positions upon cooling. There was no significant change in the tilt angle of the mean plane of the radical to the stacking direction. There was some shortening of the intra-stack contacts, but no anomalous variations could be detected amongst the shortening of inter-stack contacts (Fig. 7) throughout the temperature range studied. On cooling below 225 K, a large mosaic spread became apparent and examination of a number of crystals indicated a tendency to shatter. The apparent discrepancy between the lowest temperature of the crystallographic study of the high temperature phase [225(2) K] and the structural transition observed from other measurements described below [232–234 K] can be attributed to the errors associated with the absolute measurement of temperature on the cryostream device.[21]

Low temperature phase. Single crystal determinations of the low temperature phase were measured at 150 K on both crystals sublimed at 45 °C *in vacuo*, and on crystals grown from hexane solution. Both structures were identical. The low temperature phase of **1** crystallises in the triclinic space group $P\bar{1}$, with two molecules in the asymmetric unit. The two molecules of **1** in the asymmetric unit [Fig. 8a] have essentially identical geometries to the high temperature phase. Both are planar within 0.02 Å but there are evident differences in the crystal packing. The foremost difference is a clear disruption of the regular π-stacking motif has occured to give discrete dimers which stack along the crystallographic *c*-axis. The intradimer S···S contacts vary from 3.236 Å (S2···S2′) and 3.321 Å (S1···S1′) at the dithiazolyl ring to the longer S3···S3′ separation of 3.461 Å at the thiadiazolyl ring. The closer contacts at the dithiazolyl ring are in accord with the greater unpaired spin density at these S atoms. The asymmetric nature of these contacts also leads to a tilting of the two molecular planes, such that they are inclined at 3.5° with respect to each other. In addition to the dimerisation process, there is lateral slippage of the radical pairs away from the vertical stacking motif [Fig. 8b]. The inter-dimer contacts are S3···S(3′a) at 3.651, S1···S(1′a) at 3.774 and S2···S(2′a) at 3.848 Å along the stacking direction. It is notable that the strongest intra-dimer contacts also exhibit the weakest inter-dimer contacts along the stacking direction.

Table 3 Crystal data for **1**

T/K	310(2)	250(2)	225(2)	150(2)
Crystal size/mm	0.15 × 0.15 × 0.15	0.15 × 0.15 × 0.15	0.15 × 0.15 × 0.15	0.14 × 0.14 × 0.10
Crystal system	Monoclinic	Monoclinic	Monoclinic	Triclinic
Space group	$P2_1/c$	$P2_1/c$	$P2_1/c$	$P\bar{1}$
a/Å	9.4430(8)	9.4320(8)	9.4280(8)	6.9220(4)
b/Å	3.7170(4)	36810(3)	3.6650(3)	7.4920(7)
c/Å	15.0630(8)	15.0400(7)	15.0290(8)	9.9690(9)
α/°	90	90	90	77.564(3)
β/°	104.615(5)	104.577(5)	104.545(5)	79.209(5)
γ/°	90	90	90	83.048(5)
V/Å^3	511.60(8)	505.37(6)	502.66(7)	494.17(7)
Z	4	4	4	4
μ/mm^{-1}	1.312	1.328	1.335	1.358
Total reflections	1951	1938	1926	2681
Unique	1155	1147	1144	1725
R_{int}	0.0239	0.0215	0.0211	0.0321
$R_1(I>2\sigma(I))$	0.0349	0.0317	0.0306	0.0283
wR_2 (all data)	0.0946	0.0792	0.0792	0.0674

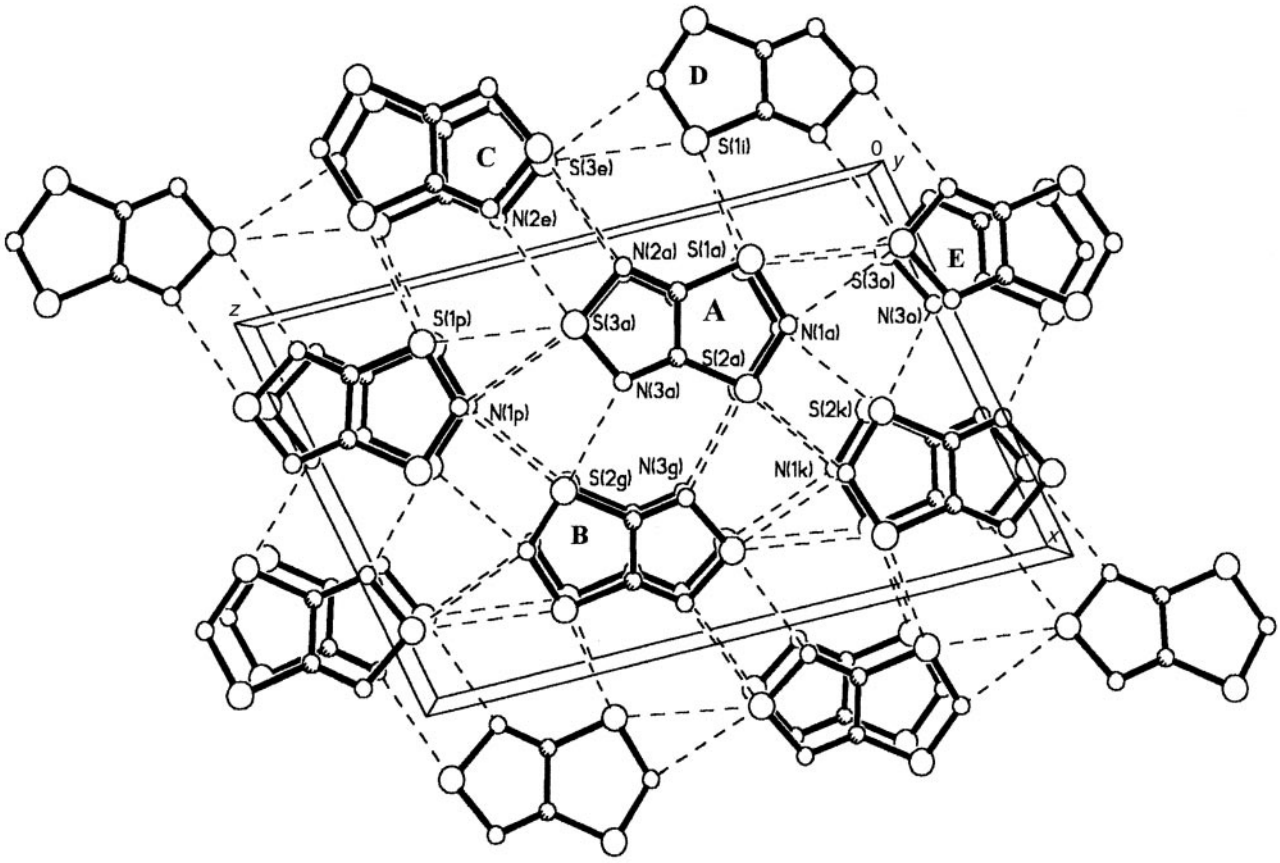

Fig. 6 Interstack contacts in the high temperature phase of **1** at 225 K. Selected intermolecular contacts are: S(1a)···S(1i) 3.371, S(1a)···S(3o) 3.614, S(2a)···N(3g) 3.031, S(2a)···N(1k) 3.237, N(1a)···S(2k) 3.237, N(1a)···S(3o) 3.138, N(2a)···S(3e) 3.115, N(3a)···S(2g) 3.031, S(3a)···N(2e) 3.115, S(3a)···S(1p) 3.614, S(3a)···N(1p) 3.138 Å.

There are a number of inter-stack contacts close to the molecular plane. Despite the crystallographic phase transition, these can be clearly related to similar contacts in the high temperature phase, although the lower symmetry gives a wider range of distances. In some circumstances the intermolecular separations are close to those anticipated from extrapolation of the high temperature structural data, *e.g.* S2···N3′ and S2′···N3 contacts at 2.923 and 2.918 Å (*cf.* monoclinic phase at 3.031 Å at 225 K) and S3···N2′ and S3′···N2 contacts at 3.056 and 3.046 Å (*cf.* monoclinic phase at 3.115 Å at 225 K). In some cases there is an alternation of contacts associated with the lattice distortion, *e.g.* S1′···S1′ at 3.304 and S1···S1 at 4.564 Å (*cf.* monoclinic phase at 3.371 Å at 225 K) and S2···N1 at 3.192 and S2′···N1′ at 3.485 Å (*cf.* monoclinic phase at 3.237 Å at 225 K). In other cases, the interstack contacts are increased on cooling to the low temperature phase, *e.g.* S3···N1 at 3.221 and S3′···N1′ at 3.340 Å (*cf.* monoclinic phase at 3.138 Å at 225 K) and S3···S1 at 3.621 and S3′···S1′ at 3.674 Å (*cf.* monoclinic phase at 3.614 Å at 225 K). With the exception of the dimerisation of the π-stack, the intermolecular contacts in both phases seem broadly comparable.

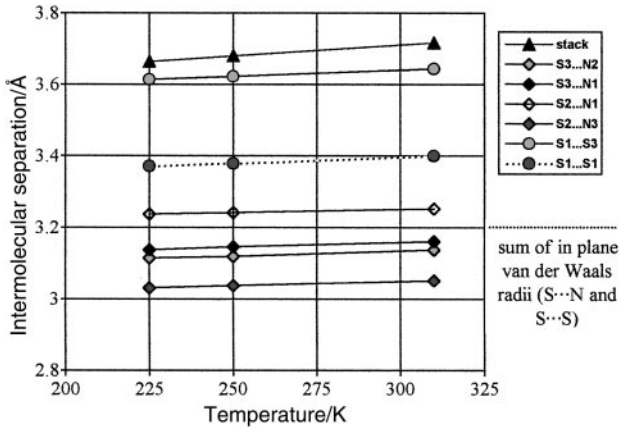

Fig. 7 Variation in intermolecular contacts in the monoclinic phase of **1** as a function of temperature.

A magnetic study of 1

DC susceptibility measurements on the high temperature phase. The monoclinic phase of **1** exhibits an effective magnetic moment of 1.0 μ_B at room temperature, significantly less than that anticipated for an $S=½$ paramagnet. A plot of χ *vs.* T shows little variation on cooling to 225 K (Fig. 9). The magnetic data for this phase (225–350 K) was modelled as a one-dimensional Heisenberg chain[22] of $S=½$ ions and yielded an intra-stack coupling of $\boldsymbol{J}=-320$ K, but required an additional interstack coupling of $z\boldsymbol{J}'=-60$ K (z = number of nearest neighbours). These values are identical to those reported by Fujita and Awaga.[12] Although the one-dimensional chain model reproduces the experimental data, the magnitude of $z\boldsymbol{J}'/\boldsymbol{J}$ ($\sim$0.2) indicates that it does not behave as a good one-dimensional system. An abrupt transition occurs on cooling below 225 K and by 200 K the paramagnetism is essentially quenched, consistent with the structural phase change already described.

DFT studies on the high temperature phase. DFT studies were carried out to assess the strength of the magnetic exchange interactions through the broken-symmetry method. The exchange interaction between pairs of neighbouring radicals were calculated through calculation of their singlet–triplet separation ($2\boldsymbol{J}$). This pair-wise interaction allows estimates of the exchange interaction energies through nearest neighbour

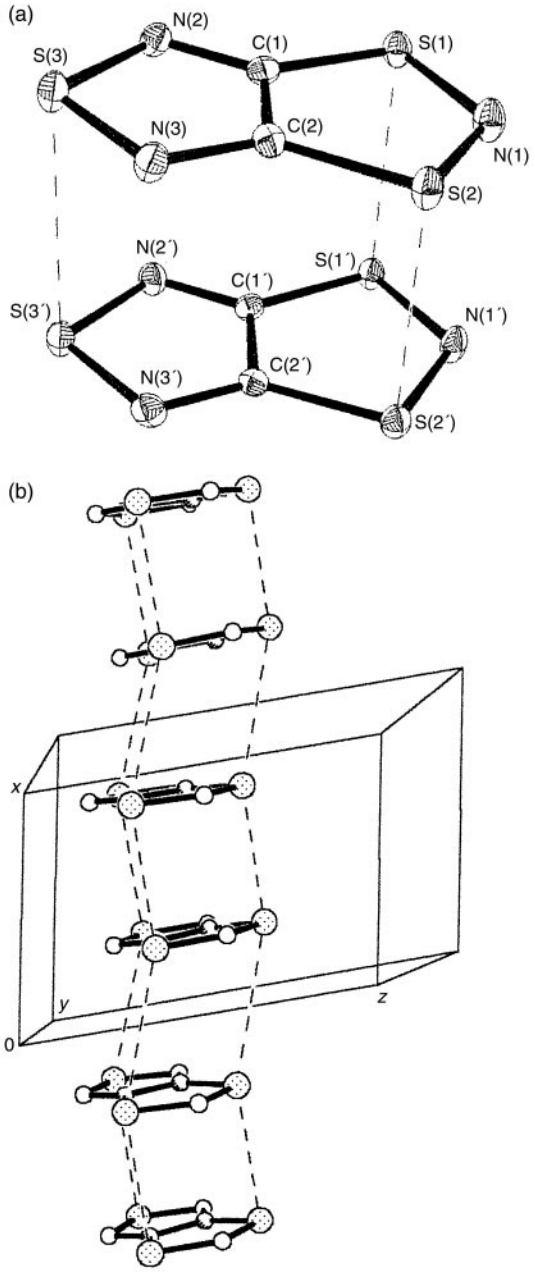

Fig. 8 (a) The asymmetric unit of **1** (triclinic phase) at 150 K and (b) Peierls distortion along the stacking direction in the low temperature phase. Selected bond lengths and angles are: S(1)–N(1) 1.655(2), S(1)–C(1) 1.735(2), S(2)–N(1) 1.651(2), S(2)–C(2) 1.735(2), S(3)–N(3) 1.649(2), S(3)–N(2) 1.652(2), N(2)–C(1) 1.320(3), N(3)–C(2) 1.319(3), C(1)–C(2) 1.433(4), S(1′)–N(1′) 1.661(2), S(1′)–C(1′), 1.734(2), S(2′)–N(1′) 1.651(2), S(2′)–C(2′) 1.735(2), S(3′)–N(2′) 1.646(2), N(2′)–C(1′) 1.322(3), N(3′)–C(2′) 1.322(3), C(1′)–C(2′) 1.435(3) Å; N(1)S(1)C(1) 98.04(11), N(1)S(2)C(2) 98.08(11), N(3)S(3)C(2) 99.27(11), S(2)N(1)S(1) 116.86(12), C(1)N(2)S(3) 105.83(17), C(2)N(3)S(3) 106.48(17), N(2)C(1)S(1) 131.9(2),C(2)C(1)S(1) 113.44(18), N(3)C(2)C(1) 113.7(2), N(3)C(2)S(2) 132.7(2), C(1)C(2)S(2) 113.58(18), N(1′)S(1′)C(1′) 98.01(11), N(1′)S(2′) C(2′) 98.07(11), N(2′)S(3′)N(3′) 99.19(11), S(2′)N(1′)S(1′) 116.81(12), C(1′)N(2′)S(3′) 106.32(17), C(2′)N(3′)S(3′) 106.41(17), N(2′)C(1′)C(2′) 114.3(2), N(2′)C(1′)S(1′) 132.3(2), C(2′)C(1′)S(1′) 113.43(18), N(3′)C(2′)C(1′) 113.8(2), N(3′)C(2′)S(2′) 132.50(19), C(1′)C(2′)S(2′) 113.67(18)°.

interactions throughout the structure. For the high temperature phase, the dominant exchange interaction was along the π-stack and estimated at $2J = -182$ K. Inter-stack interactions were one to two orders of magnitude smaller, ranging from $2J = -12$ to $+7$ K, depending on the nature of the closest contact. In Fig. 6, the lateral exchange interactions between rings **A** and **B**, **A** and **C**, **A** and **D** and **A** and **E** are $2J = -3$, -2, -12 and $+7$ K respectively. The subtle differences in the magnitude and sign of the interstack interactions reflect the difference in the nature of the contact (S···N *vs.* S···S) and the angle of contact between neighbouring rings. These values are in a good qualitative agreement with the observed data, which was modelled as a one-dimensional Heisenberg chain with $J = -320$ K and $zJ' = -60$ K. Given that each π-stack has six neighbouring stacks, then a mean value for J' is *ca.* -10 K. The asymmetry in the magnetic exchange interaction arises out of the nature of the SOMO which is of π-character. This leads to strong orbital overlap along the π-stacking direction (and hence strong intra-stack exchange), but much weaker exchange interactions between stacks.

Susceptibility measurements on the low temperature phase. The low temperature phase is diamagnetic up to 310 K. After applying a correction for the diamagnetism of both the sample holder and the sample diamagnetism, a weak paramagnetic tail could be detected. On warming the low temperature phase to room temperature, the paramagnetic susceptibility is essentially constant to 310 K but then increases abruptly, reaching the susceptibility of the original measurement (observed on the cooling cycle) at 330 K. Because of the essentially diamagnetic response throughout the temperature range, up to the phase change, the modelling of the magnetic behaviour cannot be overly reliable. Using the Bleaney–Bowers equation for an exchange-coupled dimer of $S = ½$ ions,[23] an analysis of the sample paramagnetism around 300 K indicates that the singlet–triplet separation, $2J$, must be in excess of -2071 K. This is in agreement with the value reported by Awaga ($J = -1300$ K).[12]

DFT studies on the low temperature phase. The structural phase transition leads to a displacement of molecules along the π-stacking direction, leading to alternate long and short intra-stack contacts. There are some modifications to the inter-stack contacts but these structural modifications are smaller. DFT calculations on the low temperature, dimeric, phase indicated that the ground state electronic configuration is an open shell singlet with exceptionally strong antiferromagnetic coupling between the two closely associated radicals, $2J = -2657$ K.[24] This is in contrast to many dithiadiazolyl radicals[25] and other dithiazolyl radicals[25] in which a closed-shell singlet (spin-paired dimer) is the electronic ground state. The inter-dimer magnetic exchange along the π-stacking direction is two orders of magnitude smaller ($2J = -64$ K) and the inter-stack exchange interactions are a further order of magnitude smaller, ranging from $2J = -1.4$ to -7.3 K. These interstack interactions are of a similar magnitude to those observed in the high temperature phase, although some modification is observed due to the different relative displacements of the molecules with respect to one another. Notably the interactions in this case are all antiferromagnetic. The small magnitudes of both the inter-dimer and inter-stack interactions compared to the intra-dimer interaction indicate that an exchange-coupled dimer is a good model for this system.

Susceptibility studies of the phase transition. The transition temperatures between the two phases were estimated from the maximum change in susceptibility as a function of temperature, $d\chi/dT$ (Fig. 9c). It can be clearly seen that $Tc_{\downarrow} = 234 \pm 1$ K and $Tc_{\uparrow} = 316 \pm 1$ K. These values differ slightly from those reported by Awaga (230 and 305 K respectively),[12] although it is unclear how their values were determined. Certainly both $Tc_{\downarrow}$ values reported by Awaga and from our own results are consistent within error, although the discrepancy in $Tc_{\uparrow}$ is more marked. The difference in these values is not immediately apparent, although it might be associated with crystal defects which might either suppress or enhance the phase transition temperature. Our own studies indicate that crystals of the

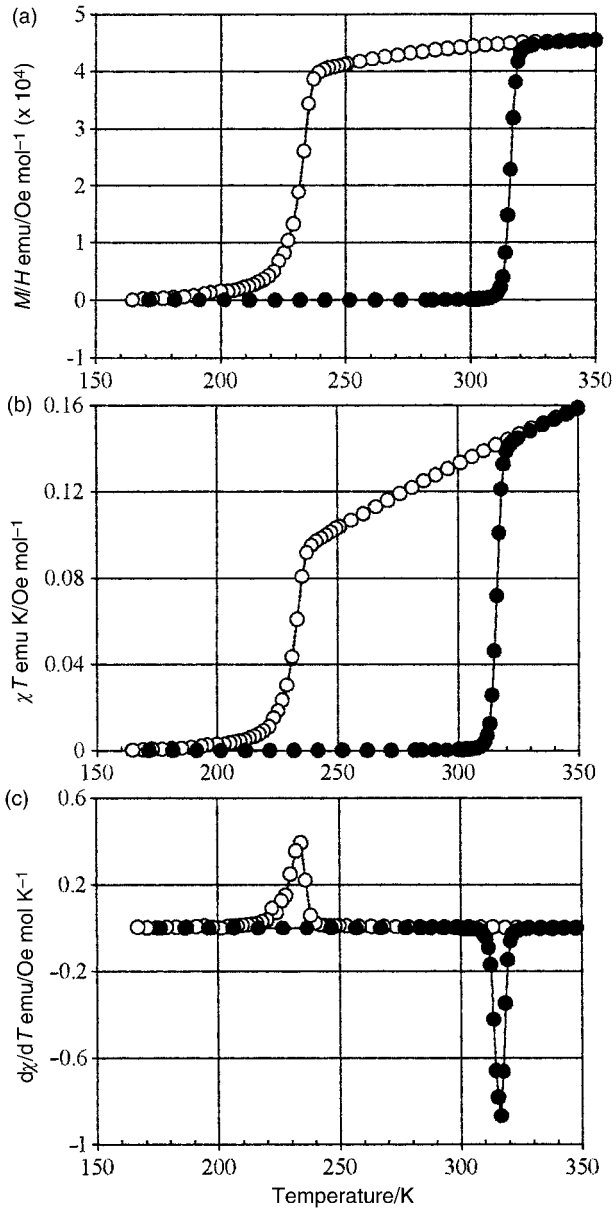

Fig. 9 (a) *M*/*H vs. T* in an applied field of 1 T; (b) μ_{eff} *vs. T* and ; (c) dχ/d*T vs. T* on cooling from 350 to 160 K (○), and then on warming from 160 to 350 K (●).

monoclinic phase have a tendency to shatter on cooling through the phase transition. However Awaga reports[12] that the sample could be cycled several times with 'little change in the hysteresis loop'. Thus whilst it might be appealing to attribute differences to sample crystallinity, an alternative explanation would appear necessary. This argument is further aggravated by noting that both the samples used in the present study and those reported by Awaga[12] were prepared by vacuum sublimation.

EPR measurements. Variable temperature X-band EPR studies (Fig. 10a) on a polycrystalline sample of **1** exhibited a similar response to the magnetic susceptibility data, with the sample producing a rapid decrease in signal intensity below 250 K although the greater sensitivity of the technique (*cf.* susceptibility measurements) indicated a residual paramagnetic component at 180 K. On warming, an increase in signal intensity became apparent above 300 K, with the original susceptibility being regained by 322 K. Analysis of the d(intensity)/d*T* curves (Fig. 10b) gives transition temperatures of $Tc_{\downarrow} = 232 \pm 1$ K and $Tc_{\uparrow} = 316 \pm 1$ K, in excellent agreement with the magnetic susceptibility data.

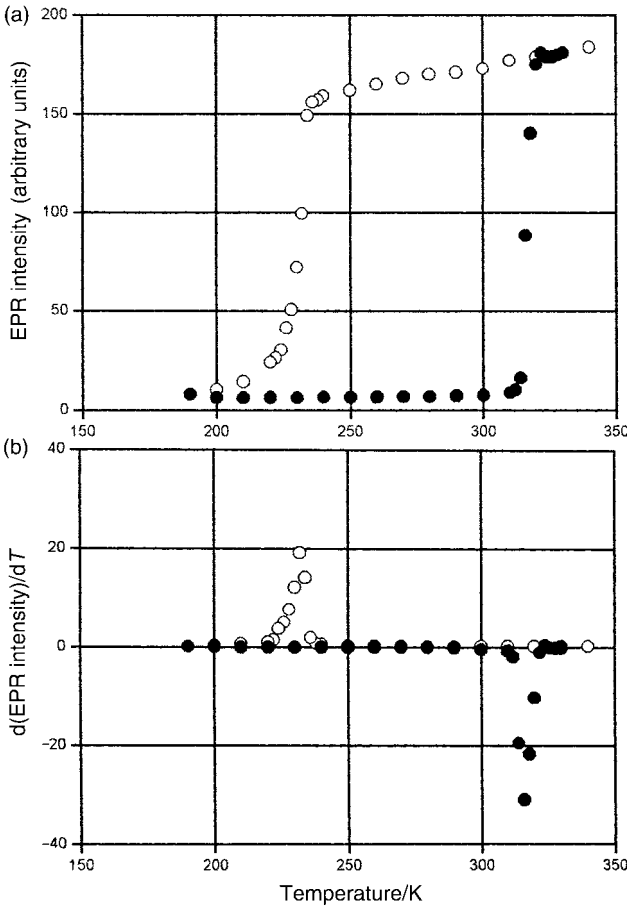

Fig. 10 Variation of (a) EPR signal intensity, ***I*** as a function of temperature and (b) d(***I***)/d*T* for a polycrystalline sample of **1**. Data for cooling and warming studies between 350 and 160 K are shown as ○ and ● respectively.

Thermodynamic studies

In order to estimate the energy associated with the phase transition, calorimetric studies were carried out on **1**. Initial adiabatic and ac calorimetry measurements proved unsuccessful with problems encountered around the transition temperature of 320.5 K. (47.3 °C). We suspect that this may be due to sample sublimation or decomposition since both are carried out under low pressure (10^{-5} mbar for adiabatic calorimetry and 10 mbar of He for ac calorimetry). The vapour pressure of **1** is sufficient for sublimation to occur slowly at room temperature and pressure [sublimation occurs more rapidly at 65 °C *in vacuo*].

Thermodynamic parameters for the phase change were eventually achieved using differential scanning calorimetry, carried out at ambient pressure. These measurements clearly illustrated the first-order nature of the phase transition and the low energy barrier to interconversion of the two phases. The transition temperatures were measured at $Tc_{\downarrow} = 232.3$ K and $Tc_{\uparrow} = 320.5$ K, in good agreement with our values measured by both magnetic susceptibility and EPR [232–234 K and 316 K]. The heating transition temperature is higher than the one reported by Fujita (305 K)[12] and also sharp. It is more consistent with our values of $Tc_{\uparrow}$ extracted from EPR and susceptibility measurements, all of which are notably higher than those previously reported. The transition is clearly first order with thermal hysteresis of 88.2 K. The low temperature transition is not as sharp as the heating one and the spread is about the same as that observed in susceptibility measurements.

The enthalpy and entropy contributions can be extracted from the DSC data and yield the following estimates:

$\Delta H_{\downarrow} = 1.41$ kJ mol^{-1}, $\Delta S_{\downarrow} = 6.0$ J mol^{-1} K^{-1} and $\Delta H_{\uparrow} = 1.86$ kJ mol^{-1}, $\Delta S_{\uparrow} = 5.8$ J mol^{-1} K^{-1}. The calculated values of ΔS are the same for both heating and cooling processes. This value is very close to $\Delta S = R\ln 2$, that would indicate an ordering process with the number of available states above Tc twice the number of states below Tc. This would be the entropy change going from diamagnetic exchange-coupled dimers to a configuration with completely disordered $S = ½$ radicals.

Discussion

Room temperature bistability between diamagnetic and paramagnetic phases of an organic radical is an important development in the generation of organic magnetic materials. The potential of switching between paramagnetic and diamagnetic phases of **1** through the application of an external stimulus (pressure, light, heat *etc.*)[12] finally provides an example of an organic radical which has the capacity for room temperature data storage. Here we discuss the key structural features inherent in **1** which lead to this phenomenon.

Polymorphism and bistability

In order to achieve bistability, there must be two polymorphs of comparable energy which can be directly transformed into each other and which exhibit a low energy barrier to interconversion. Polymorphism is not uncommon, particularly in molecular materials in which the forces between molecules are often weak (van der Waals forces, π–π interactions and hydrogen bonds).[26] Indeed a number of thiazyl-based radicals have been shown to exhibit polymorphism.[2,27] The observation of polymorphism is not, however, sufficient for a compound to exhibit bistability. In many cases, polymorphs have significantly different structural motifs and interconversion may require substantial lattice reorganisation, *e.g.* reorientation of 50% of the molecules of *p*-NCC_6F_4CNSSN by 180° would be required to interconvert between its centric α and polar β-phases.[2] In these circumstances a large energy barrier to interconversion arises [Fig. 11b] or no pathway directly connects the two polymorphs. Thus the structures may be polymorphic but not bistable. In the case of **1**, DSC studies indicate that the dimeric, low temperature phase is marginally more thermodynamically stable ($\Delta H \sim 1.5$ kJ mol^{-1}) than the high temperature phase. In addition, a comparison of the two structures indicate that minimal lattice reorganisation is required for interconversion and so bistability becomes feasible.

It is a non-trivial task to separate the different contributions to bonding (electrostatic interactions, exchange interactions and dispersion forces) within molecules. However, in the case of π-stacked arrangements such as **1**, and the related heterocycle, $C_4S_3N_5$,[10] the bonding can be conveniently separated into two components: intra- and inter-stack interactions. In the case of the intra-stack interactions, significant orbital overlap of SOMOs is possible and SOMO–SOMO bonding interactions are liable to contribute significantly to this component of the lattice energy. In contrast, inter-stack interactions in **1** are likely to possess a significant electrostatic contribution, with notable $S^{\delta+}\cdots N^{\delta-}$ interactions evidenced by the molecular electrostatic potential map (Fig. 3b). Inter-stack bonding interactions between singly occupied MO's are likely to be minimal.

Bistability in dithiazolyl and dithiadiazolyl radicals

The Peierls distortion of a regular spaced π-stack leads to sets of short and long contacts along the stacking direction.[28] To a first approximation, we can consider this as a dimerisation process. In order to inhibit this dimerisation, inter-stack interactions of a similar energy to the dimerisation process are needed.

Solution EPR studies on related dithiazolyls[6] have shown that the π–π dimerisation process is ~ 0 kJ mol^{-1} *i.e.* solvation effects balance the tendency for dimerisation. Indeed in the solid state, a number of dithiazolyl radicals are monomeric[15] and the tendency for dimerisation in π-stacked derivatives is inhibited by inter-stack interactions. In contrast, the isoelectronic dithiadiazolyl radicals,[5] RCNSSN exhibit a large

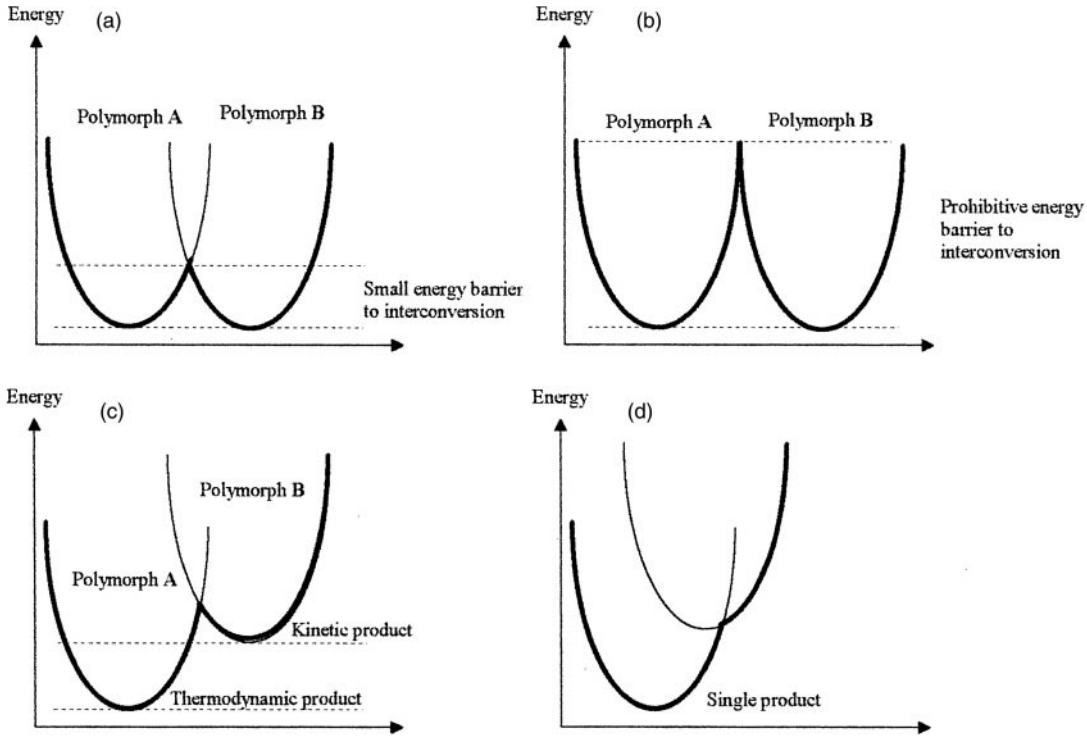

Fig. 11 Potential wells for (a) bistability; (b) distinct polymorphism without bistability; (c) polymorphism with kinetic and thermodynamic products; (d) loss of polymorphism due a lowering of the energy barrier to interconversion.

dimerisation energy in solution ($\Delta H_{dim} \sim 35$ kJ mol^{-1}) and it is perhaps unsurprising that these radicals invariably form dimeric π-stacks.[28] [The regular π-stacked structure[29] of 2,5-$F_2C_6H_3CNSSN$ has recently been re-investigated and found to be a dimeric π-stack[30]]. In this case the relative energies of the two polymorphs (monomer and dimer) may be expected to be substantially different [Fig. 11c] with the dimeric form of considerably lower energy than the regular π-stacked motif.

If the energy barrier to interconversion becomes too small, or the double minimum in the potential energy surface completely disappears then only one 'polymorph' is observed [Fig. 11d]. The fine tuning of this energy barrier, and the relative depths of the potential wells are the key to control bistability.

Conclusion

The electronic structure of the thiazyl radical, **1**, has been probed by a combination of EPR spectroscopy and DFT calculations. These indicate delocalisation of the unpaired spin density over the entire molecule. Radical **1** crystallises in two interconvertable morphologies and the interconversion has been examined by XRPD, DSC, EPR and magnetic susceptibility measurements. All techniques indicate that **1** exhibits a broad thermal hysteresis ($Tc_{\downarrow} = 234$ K, $Tc_{\uparrow} = 317$ K) with bistability clearly apparent at room temperature. The bistability has been attributed to a first order, structural phase transition between a regular π-stacked arrangement of radicals (monoclinic $P2_1/c$) and a dimeric π-stack with alternating short and long contacts (triclinic, $P\bar{1}$). There is no evidence for any intermediate ternary phase.

An analysis of the magnetic behaviour of the high temperature phase through magnetic measurements and DFT studies indicate strong antiferromagnetic exchange interactions ($J = -320$ K) along the **π**-stacking direction, with weaker but significant interactions between stacks. In contrast the low temperature phase can be considered as a strongly coupled dimer in which the exchange interaction is so strong ($2J = -2657$ K) as to render the sample essentially diamagnetic.

The bistability in **1** is attributed to an energetic match of the inter-stack interactions with the tendency of the π-stack to undergo a Peierls distortion. The temperature range of the bistability provides the opportunity to study magnetic switching in an organic radical at room temperature. Whilst the current results are in broad agreement with those previously reported, a significant difference in the temperature range for bistability is observed. The determination of $Tc_{\uparrow}$ from three different experimental methods provided a value of $Tc_{\uparrow}$ which is consistently 10–15 K greater than that reported by Awaga.[12] The discrepancy between the two sets of results is beyond experimental error and warrants further investigation. Preliminary studies indicate that neither the method of sample preparation nor sample crystallinity appear to be contributing factors to this anomaly. A number of additional studies are underway.

Experimental

Materials and methods

Sulfur dichloride (BDH) was distilled prior to use. Dithiooxamide (Aldrich), sodium dithionite (Aldrich), sulfuryl chloride (BDH) and trimethylsilyl amide (Aldrich) were used without further purification.

Mass spectra (EI+) were recorded on a Kratos MS890 mass spectrometer. Microanalyses were performed using an Exeter CE-440 elemental analyser.

Preparation of $[C_2S_3N_3]Cl$. SCl_2 (1.8 g, 17.4 mmol) was added to a solution of dithiooxamide (2.0 g, 16.7 mmol) in THF (40 ml) stirred at 0 °C. An orange precipitate formed immediately and the solution was stirred at room temperature for a further 2 hours. The solid was filtered, washed with THF (2×20 ml) and dried *in vacuo* to yield crude 4,5-disulfanyl-1,2,5-thiadiazole. SO_2Cl_2 (1.89 g, 14 mmol) was added to a stirred suspension of crude 4,5-disulfanyl-1,2,5-thiadiazole (1 g, 6.7 mmol) in CH_2Cl_2 (40 ml) and refluxed for 2 hours giving a red solution. The solvent and excess SO_2Cl_2 were removed *in vacuo* to give a red oil. This oil was dissolved in CH_2Cl_2 (15 ml) and stirred at 0 °C whilst a solution of trimethylsilyl azide (0.77 g, 6.7 mmol) in CH_2Cl_2 (10 ml) was added dropwise forming a brown precipitate of $[C_2S_3N_3]Cl$. The solution was stirred overnight, then filtered and the orange–brown solid washed with CH_2Cl_2 (2×10 ml) and dried *in vacuo* (yield 515 mg, 39%) (Found: C, 12.9; H, 0.0; N, 21.0. Calc: C, 12.2; H, 0.0; N, 21.3%).

Preparation of $C_2S_3N_3$. Sodium dithionite (11 g, 0.1 mol) and $[C_2S_3N_3]Cl$ (1.28 g, 6.5×10^{-3} mol) were stirred together in acetonitrile (20 ml). 40–60 °C Petroleum ether (20 ml) was layered on top of the reaction mixture. After a few minutes, stirring was stopped and the blue ether phase was removed by canula transfer and replaced by fresh ether; this procedure was continued until the ethereal phase remained colourless. The combined extracts were evaporated to dryness and the solid residue sublimed *in vacuo* in a sealed tube (60 °C, 10^{-2} Torr) to give dark rhombs (320 mg, 30%). Found: C, 14.8; N, 25.5%, Calc: C, 14.8; N, 25.9%; *m/z* (EI+) 161.9 (M^+, 100%).

X-Ray diffraction studies. X-Ray powder diffraction patterns were recorded on a Stoe-Stadi P diffractometer with Cu-Kα_1 radiation using a curved Ge monochromator and linear PSD, operating in Debye–Scherrer mode at room temperature. The patterns were fitted using the Le Bail method[31] and Fulprof.[32] A polycrystalline sample was sealed in a 0.5 mm o.d. capillary and patterns recorded on the as-prepared sample, after quenching the capillary in liquid nitrogen (77 K) and after heating at 55 °C (328 K) in a Kugelruhr for 20 minutes.

Single crystal X-ray diffraction studies were carried out on a Nonius Kappa-4 CCD diffractometer, using Mo-Kα radiation and equipped with an Oxford Instruments Cryostream. A crystal of the triclinic phase was mounted on the end of a glass fibre with fluoropolymer, whilst the variable temperature studies on the monoclinic phase of **1** were all carried out on a single crystal mounted on the end of a glass fibre with Araldite. Data collection, reduction and cell refinement employed DENZO and COLLECT software.[33,34] An absorption correction was applied using SORTAV.[35] Crystal structure solution was achieved with SHELXS97 and refined with full matrix least squares on F^2 with SHELXL97.[36] All atoms were refined anisotropically. Crystallographic data and refinement parameters for **1** are given in Table 3. CCDC reference number 158385–158388. See http://www.rsc.org/suppdata/jm/b1/b103303b/ for crystallographic files in .cif format.

Magnetic and EPR measurements. Magnetic measurements were made on a Quantum Design SQUID magnetometer in the range 160–350 K in an applied field of 1 T. The data shown in Fig. 5 are corrected for diamagnetism, using the observed sample diamagnetism (0.80486×10^{-4} emu mol^{-1}) at low temperature. EPR spectra were recorded on a Bruker EMX (X-band) and Bruker ESP 300E (K-band) spectrometers. Spectrum simulations were achieved using in-house software.[37]

Calorimetry studies. DSC studies were made on a Perkin-Elmer DSC7, using heating and cooling rates of 10 K min^{-1}. The system was calibrated for the temperature and enthalpy scales with standard samples and a detailed heat capacity calibration measurement made with aluminium sapphire. Data

were collected for an empty aluminium capsule prior to sealing the sample in the same capsule. The sample measurements were corrected for the empty capsule. Values of $Tc_{\downarrow}$ and $Tc_{\uparrow}$ were taken from extrapolations of the peak increasing ramps.[38] The values of ΔH and ΔS are calculated as the integral of $C.\mathrm{d}T$ (by definition) and as $C/T.\mathrm{d}T$ (thermodynamically equivalent) respectively. For convention, the sign for the enthalpy and entropy parameters for the transitions are quoted for increasing temperature.

DFT studies. The theoretical value of $\boldsymbol{J}$ was computed within the broken symmetry approximation of the density functional approach,[39] by taking the difference between the energy of the symmetry broken ground state singlet and the energy of the triplet ground state. Such methodology has been shown to give accurate descriptions of the values of J on organometallic[40] and molecular systems.[41] The energy for the singlet was taken to be that from the broken symmetry computation, following the recent results which suggest that this is the correct procedure.[42] Both of these energies were computed using the B3LYP non-local exchange and correlation functional,[43] and the LANL2DZ basis set[44] which uses effective core potentials to describe the inner electrons while the outer s and p electrons are described using a gaussian double zeta basis set. The geometries employed in the computations were taken directly from the crystal data.

Acknowledgements

We would like to thank the EPSRC for a studentship (GDM), the Royal Society for an equipment grant (JMR) and the CICYT for grant MAT97-0951 (FP and PO). This work was also supported by the Materials Program of the Comision Interministerial de Ciencia y Technologia under grant MAT97-987 and PB98-1166-C02-02 and by CIRIT (grant 1999SCG 00046). the computational time was provided by CESCA/CEPBA. We thank Mr John Friend (EPSRC c.w. EPR Service Centre) for some of the EPR measurements.

References

1 See for example: J. M. Rawson and F. Palacio, 'Magnetic Properties of Thiazyl Radicals' in *π-Electron Magnetism*, ed. J. Veciana, Springer-Verlag in the press; G. Antorrena, N. Bricklebank, F. Palacio, J. M. Rawson and J. N. B. Smith, *Phosphorus Sulfur Silicon Relat. Elem.*, 1997, **124–125**, 133; J. M. Rawson, R. J. Less, J. N. B. Smith, F. Palacio and G. Antorrena, *Mol. Cryst. Liq. Cryst.*, 1999, **334**, 275.

2 A. J. Banister, N. Bricklebank, W. Clegg, M. R. J. Elsegood, C. I. Gregory, I. Lavender, J. M. Rawson and B. K. Tanner, *J. Chem. Soc., Chem. Commun.*, 1995, 679; A. J. Banister, N. Bricklebank, I. Lavender, J. M. Rawson, C. I. Gregory, B. K. Tanner, W. Clegg, M. R. J. Elsegood and F. Palacio, *Angew. Chem., Int Ed. Engl.*, 1996, **35**, 2533; F. Palacio, G. Antorrena, M. Castro, R. Burriel, J. M. Rawson, J. N. B. Smith, N. Bricklebank, J. Novoa and C. Ritter, *Phys. Rev. Lett.*, 1997, **79**, 2336; F. L. Pratt, A. E. Goeta, F. Palacio, J. M. Rawson and J. N. B. Smith, to be published.

3 G. Antorrena, J. E. Davies, M. Hartley, F. Palacio, J. M. Rawson, J. N. B. Smith and A. Steiner, *Chem. Commun.*, 1999, 1393; P. J. Alonso, G. Antorrena, J. I. Martinez, J. J. Novoa, F. Palacio, J. M. Rawson and J. N. B. Smith, *Appl. Magn. Reson.*, 2001, **20**, 231.

4 R. J. Less, J. M. Rawson, M. Mito, S. Takagi, H. Deguchi, K. Takeda and F. Palacio, manuscript in preparation.

5 S. A. Fairhurst, K. M. Johnson, L. H. Sutcliffe, K. F. Preston, A. J. Banister, Z. V. Hauptman and J. Passmore, *J. Chem. Soc., Dalton Trans.*, 1986, 1465.

6 E. G. Awere, N. Burford, R. C. Haddon, S. Parsons, J. Passmore, J. V. Waszczak and P. S. White, *Inorg. Chem.*, 1990, **29**, 4821; E. G. Awere, N. Burford, C. Mailer, J. Passmore, M. J. Schriver, P. S. White, A. J. Banister, H. Oberhammer and L. H. Sutcliffe, *J. Chem. Soc., Chem. Commun.*, 1987, 66.

7 G. D. McManus, J. M. Rawson, N. Feeder, F. Palacio and P. Oliete, *J. Mater. Chem.*, 2000, **10**, 2001.

8 T. M. Barclay, A. W. Cordes, R. H. de Laat, J. D. Goddard, R. C. Haddon, D. Y. Jeter, R. C. Mawhinney, R. T. Oakley, T. T. M. Palstra, G. W. Patenaude, R. W. Reed and N. P. C. Westwood, *J. Am. Chem. Soc.*, 1997, **119**, 2633; E. Dormann, M. J. Nowak, K. A. Williams, R. O. Angus Jr. and F. Wudl, *J. Am. Chem. Soc.*, 1987, **109**, 2594; G. Wolmershauser, G. Wortmann and M. Schnauber, *J. Chem. Res. S*, 1988, 358; G. Wolmershauser, M. Schnauber, T. Wilhelm and L. H. Sutcliffe, *Synth. Met.*, 1986, **14**, 239.

9 T. M. Barclay, A. W. Cordes, N. A. George, R. C. Haddon, R. T. Oakley, T. T. M. Palstra, G. W. Patenaude, R. W. Reed, J. F. Richardson and H. Zhang, *Chem. Commun.*, 1997, 873.

10 T. M. Barclay, A. W. Cordes, N. A. George, R. C. Haddon, M. E. Itkis, M. S. Mashuta, R. T. Oakley, G. W. Patenaude, R. W. Reed, J. F. Richardson and H. Zhang, *J. Am. Chem. Soc.*, 1998, **120**, 352.

11 G. Wolmershauser and R. Johann, *Angew. Chem., Int. Ed., Engl.*, 1989, **28**, 920.

12 W. Fujita and K. Awaga, *Science*, 1999, **286**, 261.

13 Y.-L. Chung, J. P. B. Sandall, L. H. Sutcliffe, H. Jolly, K. F. Preston, R. Johann and G. Wolmershauser, *Magn. Reson. Chem.*, 1991, **29**, 625.

14 Similar in origin to "overshoot" features commonly observed in X-band spectra of Cu(II) complexes, and arising from the combination of a relatively large *g*-anisotropy and a significant hyperfine coupling to one of the *g*-values. See F. E. Mabbs and D. Collison, *Electron Paramagnetic Resonance of Transition Metal Compounds*, Elsevier, Amsterdam, 1992, pp. 244.

15 see J. M. Rawson and G. D. McManus, *Coord. Chem. Rev.*, 1999, **189**, 135, and references therein.

16 J. M. Rawson, A. J. Banister and I. Lavender, *Adv. Heterocycl. Chem.*, 1995, **62**, 137, and references therein.

17 see for example: J. M. Rawson, A. J. Banister and I. May, *Magn. Reson. Chem.*, 1994, **32**, 487; E. G. Awere, J. Passmore, K. F. Preston and L. H. Sutcliffe, *Can. J. Chem.*, 1988, **66**, 1776.

18 J. R. Morton and K. F. Preston, *J. Magn. Reson.*, 1978, **30**, 577.

19 J. Gassmann and J. Fabian, *Magn. Reson. Chem.*, 1996, **34**, 913.

20 S. C. Nyburg and C. H. Faerman, *Acta. Crystallogr., Sect. B.*, 1985, **41**, 274.

21 The measuring temperature a few mm from the end of the cryostream [225(2) K] is, within 3 esd's, almost identical to the transition temperature measured by DSC [232.3 K]. The absolute measurement of temperature is extremely difficult in the heterogeneous environment of a open cold nitrogen stream. Indeed calibration of the cold stream temperature is recommended to be carried out by studies on compounds exhibiting known phase transitions whose transition temperature has been determined by other methods. For further details see: Operating Manual for the Cryostream Cooler version 3.1A, 1992.

22 W. E. Esters, D. P. Gavel, W. E. Hatfield and D. J. Hodgson, *Inorg. Chem.*, 1978, **17**, 1415.

23 B. Bleaney and K. D. Bowers, *Proc. Roy. Soc. (London) Ser. A.*, 1952, **214**, 451.

24 A full theoretical analysis of the magnetic exchange interaction and the relative energies of closed shell singlet, open shell singlet and the open shell triplet will be the subject of a future report.

25 A. W. Cordes, C. D. Bryan, W. M. Davis, R. H. de Laat, S. H. Glarum, J. D. Goddard, R. C. Haddon, R. G. Hicks, D. K. Kennepohl, R. T. Oakley, S. R. Scott and N. P. C. Westwood, *J. Am. Chem. Soc.*, 1993, **115**, 7232.

26 J. S. Miller, *Adv. Mater.*, 1998, **10**, 1553; J. D. Dunitz and J. Bernstein, *Acc. Chem. Res.*, 1995, **28**, 193.

27 A. W. Cordes, R. C. Haddon, R. G. Hicks, R. T. Oakley and T. T. M. Palstra, *Inorg. Chem.*, 1992, **31**, 1802; A. W. Cordes, R. C. Haddon, R. G. Hicks, R. T. Oakley, T. T. M. Palstra, L. F. Schneemeyer and J. V. Waszczak, *J. Am. Chem. Soc.*, 1992, **114**, 1729; C. D. Bryan, A. W. Cordes, R. C. Haddon, R. G. Hicks, D. K. Kennepohl, C. D. McKinnon, R. T. Oakley, T. T. M. Palstra, A. S. Perel, S. R. Scott, L. F. Schneemeyer and J. V. Waszczak, *J. Am. Chem. Soc.*, 1994, **116**, 1205.

28 For references on Peierls distortions of π-stacked thiazyl radicals, see: A. W. Cordes, R. C. Haddon and R. T. Oakley, *Adv. Mater.*, 1994, **6**, 798; C. D. Bryan, A. W. Cordes, R. M. Fleming, N. A. George, S. H. Glarum, R. C. Haddon, C. D. MacKinnon, R. T. Oakley, T. T. M. Palstra and A. S. Perel, *J. Am. Chem. Soc.*, 1995, **117**, 6880.

29 A. J. Banister, A. S. Batsanov, O. G. Dawe, P. L. Herbertson, J. A. K. Howard, S. Lynn, I. May, J. N. B. Smith, J. M. Rawson,

T. E. Rogers, B. K. Tanner, G. Antorrena and F. Palacio, *J. Chem. Soc., Dalton Trans.*, 1997, 2539.
30 L. Beer, A. W. Cordes, D. J. T. Myles, R. T. Oakley and N. J. Taylor, *Cryst. Eng Comm.*, 2000, 20.
31 A. Le Bail, H. Durog and J. L. Fourquet, *Mat. Res. Bull.*, 1998, **23**, 447.
32 J. Rodriguez-Caravajal, *Physica B*, 1993, **192**, 55.
33 DENZO: Z. Otwinowski and W. Minor, *Methods. Enzymol.*, 1997, **276**, 307.
34 COLLECT: R. Hooft, Nonius BV, Delft, Netherlands (1998).
35 R. H. Blessing, *Acta. Crystallogr., Sect. A*, 1995, **A51**, 33.
36 G. M. Sheldrick, SHELXS97 and SHELXL97, 1997, University of Gottingen, Germany.
37 Detailed in F. E. Mabbs and D. Collison, *Electron Paramagnetic Resonance of d Transition Metal Compounds*, Elsevier, Amsterdam, 1992, ch. 7.
38 In first order transitions there are discontinuous enthalpy changes at the transition temperatures. However the experimental system can not provide infinite power and there is also finite thermal conduction from sample-holder to sample which gives a constant slope in the transition peak that can be extrapolated back to the real transion temperature.
39 L. Noodleman and E. J. Baerends, *J. Am. Chem. Soc.*, 1984, **106**, 2316.
40 E. Ruiz, P. Alemany, S. Alvarez and J. Cano, *J. Am. Chem. Soc.*, 1997, **119**, 1297.
41 M. Deumal and J. J. Novoa, to be submitted.
42 J. A. Pople, P. M. Gill and N. C. Handy, *Int. J. Quantum Chem.*, 1995, **56**, 303; J. Grafenstein, A. M. Hjerpe, E. Kraka and D. Cramer, *J. Phys. Chem. A.*, 2000, **104**, 1753.
43 A. D. Becke, *J. Chem. Phys.*, 1996, **104**, 1040.
44 P. J. Hay and W. R. Wadt, *J. Chem. Phys.*, 1985, **82**, 270.